V European Conference on Computational Fluid Dynamics
ECCOMAS CFD 2010
J. C. F. Pereira and A. Sequeira (Eds)
Lisbon, Portugal,14-17 June 2010

STUDY AND CONTROL OF THE VORTICAL FLOW OVER A 65 DEGREES SWEEP DELTA WING IN THE TRANSONIC REGIME

Jacques Riou*, Eric Garnier† and Claude Basdevant††

*ONERA,
Applied Aerodynamics Department, 8 rue des Vertugadins, 92190, Meudon, France.
e-mail: jacques.riou@onera.fr
†ONERA,
Applied Aerodynamics Department, 8 rue des Vertugadins, 92190, Meudon, France.
††Institut Galilée,
Université Paris 13, 93430 Villetaneuse, France

Key words: Vortical Flow, Transonic Regime, Flow Control

Abstract. *The aim of this study is to investigate compressibility effects on the vortical flow developing over the VFE-2 delta wing and to control this flow in the transonic regime. The wing is equipped with a sharp leading-edge and presents a sweep angle of 65 degrees. The angle of attack is set to 25.5 degrees and two different Mach numbers are considered:* $M_\infty = 0.4$ *and* $M_\infty = 0.8$*. The simulations are based on a turbulent modeling coupling DDES and ZDES approaches. It is shown in a first time that compressibility impacts the dynamic of the whole vortical flow and leads to an earlier vortex breakdown in the transonic regime. Then, suction is applied on the leading-edge of the wing in the transonic regime. Such an approach allows to stabilize the leading-edge vortex and to decrease the aerodynamic loadings fluctuations. Moreover, an increase in the aerodynamic performances is observed.*

1 Introduction

Flows over delta wings are characterized by the separation of the flow coming from the pressure side. It has been experimentally demonstrated that the location of the flow separation depends on the shape of the leading-edge [1]. In the case of a rounded leading-edge, the position of the separation depends on both Reynolds and Mach numbers [2, 3] whereas it necessarily occurs at the leading-edge in the case of a sharp one. The shear layer resulting from this separation curves and curls itself to create the leading-edge vortex over the suction side of the wing.
The vortex core is the place of an intense acceleration of the longitudinal flow [4, 5], inducing a pressure decrease which contributes to the lift of the wing [6].
Nevertheless, under the influence of internal and external instabilities, the leading-edge vortex undergoes an abrupt disorganization characterized by a dilation of the vortex core,

the presence of a stagnation point on the vortex axis and an increase of turbulence levels. The occurrence of this phenomenon, known as vortex breakdown [7], can be triggered by an increase of the adverse pressure gradient or of the initial vortex circulation. The main harmful consequences of the vortex breakdown are an increase of the buffeting on the suction side of the wing and the loss of the vortical lift.
The first objective of this study is to evaluate compressibility effects on these features and the second one is to propose an efficient control approach to enhance the aerodynamic performances of the wing in the transonic regime. Particularly, efficient strategies in the subsonic regime will be assested in the transonic one.
The current investigation lies on the study of the flow over the VFE-2 wing used in the RTO-AVT-113 project [8]. This wing presents a sweep angle equal to 65 degrees and a root chord c of 0.4905 m. The sharp leading-edge configuration has been chosen since the location of the flow separation is fixed by the geometry and does not depend then on the Reynolds number. Finally, the angle of attack α is set equal to 25.5° and the Reynolds number based on the root chord of the wing is equal to $Re_c = 2 \times 10^6$. For such an angle of attack, the vortex breakdown occurs for the two considered Mach numbers. A perspective view of the model is given in figure 1.

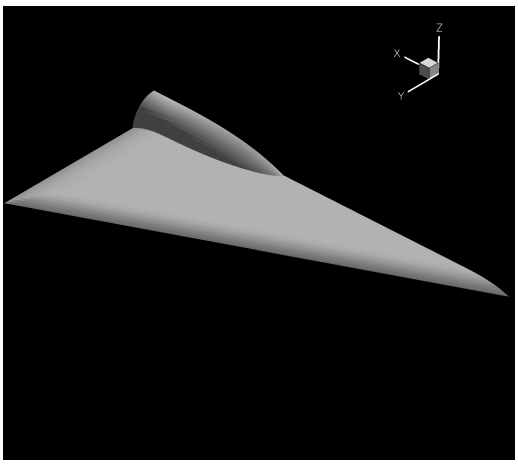

Figure 1: Perspective view of the VFE-2 delta wing.

2 Experimental reference and numerical method

2.1 Experimental reference

The vortical flows in subsonic and transonic regime over the VFE-2 delta wing have been experimentally investigated at the DLR center of Göttingen by Konrath *et al.* [9, 10, 11] and Schroder *et al.* [12].

In order to obtain the pressure distribution on the suction side, the VFE-2 delta wing had been coated with PSP (Pressure Sensitive Paint) and numerous probes were used to record the static pressure. Moreover, the flowfields have been investigated using the stereo-PIV approach in several transverse planes

2.2 Numerical method

2.2.1 The FLU3M solver

The computations presented in this article have been performed using the FLU3M solver, developed at ONERA [13]. This code is based on a cell centered finite volume technique and structured multiblock meshes. For efficiency, an implicit time integration is employed to deal with the very small grid size encountered near the wall. The time integration is carried out by means of the second-order-accurate backward scheme of Gear [14] and the time-step is set equal to 5×10^{-7}s. Moreover, four sub-iterations are used in the Newton integration. The spatial scheme is the one proposed by Mary and Sagaut [15] . It is based on the second-order-accurate AUSM+(P) scheme, whose dissipation is proportional to the local fluid velocity. Furthermore, a second-order-accurate centered scheme is used to compute the viscous fluxes.

2.2.2 Turbulent modeling

Because of the high Reynolds number of the flow preventing the use of LES or DNS, a hybrid RANS/LES method has been chosen to carry out the computations. The chosen technique relies on a coupling of the DDES method [16] with the ZDES one [17], both being grounded on the Spalart-Allmaras model [18]. This coupling is based on the f_a function of the DDES method, a threshold value f_{a0} of this function marking the external edge of the boundary layer [19].

2.2.3 Mesh description

The grid is composed of 84 domains, the number of points is 23×10^6 and the mesh is locally refined in the region of the vortical flow in order to ensure an efficient discretization of the shear layer and of the vortices, as represented in Figure 2.

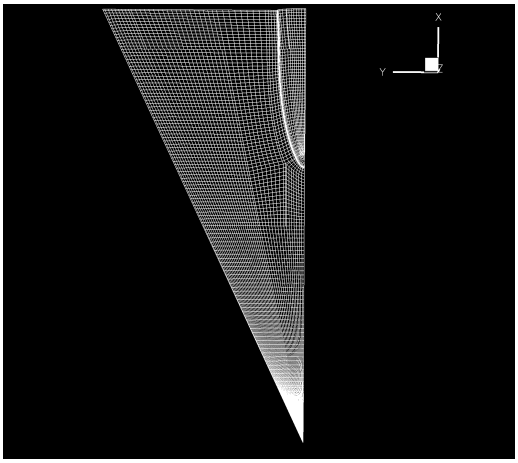

Figure 2: View of the mesh on the upper side of the VFE-2 delta wing (only one point every four in each direction).

3 Instantaneous flows and time-averaged flows validation

3.1 Analysis of the instantaneous flows

Figure 3 represents contours of $\|grad(\rho)\|$ in a plane perpendicular to the longitudinal direction located at $x/c = 0.5$. In these figures, b denotes the local half-span of the wing.

In the subsonic case, the flow detaches at the sharp leading-edge, resulting in the forma-

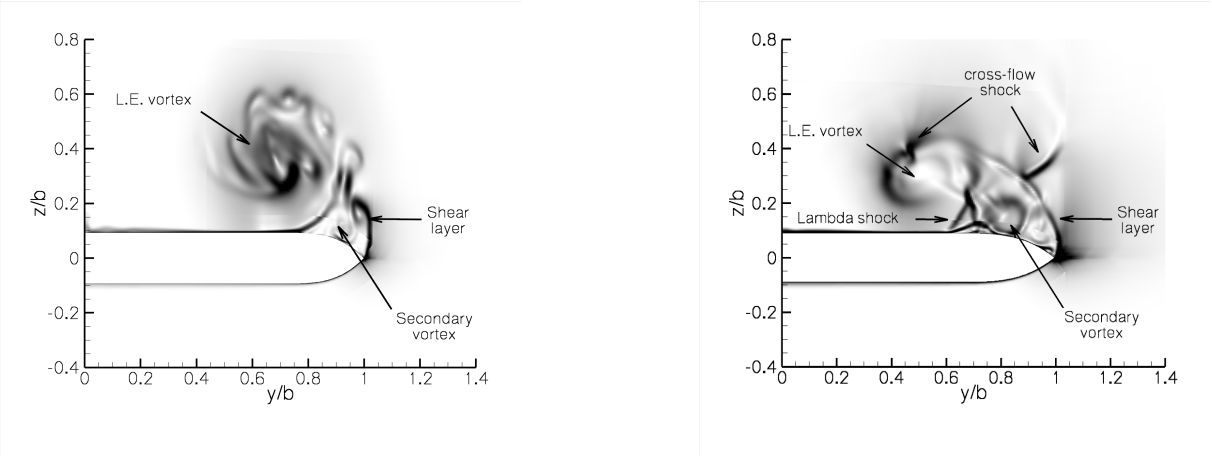

(a) (b)

Figure 3: Contours of $\|grad(\rho)\|$ in a plane perpendicular to the streamwise direction located at $x/c = 0.5$. Left: $M_\infty = 0.4$; Right: $M_\infty = 0.8$.

tion of a shear layer. Owing to the Kelvin-Helmholtz instability, vortical structures are generated in this region of the flow. These structures feed with vorticity the leading-edge vortex.
The flow topology is quite different in the transonic case. Indeed, as in the case of two-dimensional shear layers in transonic and supersonic regimes [20], the shape of the vortical structures embedded in the shear layer is altered in comparison with the subsonic case.
Finally, in the transonic case, several regions of high values of $\|grad(\rho)\|$ are identified. The two first ones are located on the top of the shear layer. Moreover, a complex shock-waves system is located beneath the leading-edge vortex. The presence of this lambda shock deeply alters the local flow topology. Owing to the interaction of this shock with the boundary layer developing on the upper side of the wing, the flow detaches and feeds the secondary vortex. It results in a larger and stronger secondary vortex than for $M_\infty = 0.4$.

3.2 Time-averaged flow validation

As it has been previously mentioned, compressibility effects on the vortical flow developing over the VFE-2 delta wing has been experimentally studied by Konrath *et al.* [9, 10, 11] and Schroder *et al.* [12] using PSP and PIV techniques.
Figures 4 and 5 show contours of $\frac{u}{U_\infty}$ and $\frac{u_\theta}{U_\infty}$, where u_θ is the tangential velocity, experimentally and numerically obtained at $\frac{x}{c} = 0.5$ for the two considered Mach numbers.

In a first time, it can be observed that the time-averaged contours of $\frac{u}{U_\infty}$ and $\frac{u_\theta}{U_\infty}$ numerically obtained are in a good agreement with the experimental data.
As previously mentioned, an increase of the freestream Mach number results in a modification of the shape of the leading-edge vortex, both in experimental and numerical results. Indeed, similarly to the experimental observations of Erickson *et al.* [21, 22], the leading-edge vortex presents a "kidney-shape" for $M_\infty = 0.8$, whereas the vortex remains circular in the subsonic regime.
These figures also illustrate that values of the tangential velocity are close to the ones of the longitudinal velocity component in the two cases. As it will be studied in a following section, it has an important influence on the dynamic of the leading-edge vortex.
Finally, in the transonic case, the distribution of u_θ is altered by the presence of the two cross-flow shocks on the top of the shear layer.

4 Overview on the leading-edge vortex

Figure 6 represents the evolution of the time-averaged longitudinal velocity $\frac{u}{U_\infty}$ in the leading-edge vortex core as a function of $\frac{x}{c}$ for the two cases.
From the apex of the wing to $\frac{x}{c} = 0.2$, the flow is characterized by an increase of the longitudinal velocity in the two vortex cores. Downstream from $\frac{x}{c} = 0.2$, the flowfield in

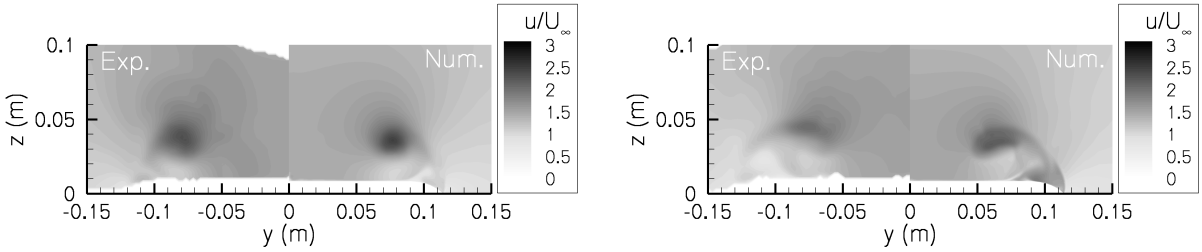

(a) (b)

Figure 4: Numerical and experimental contours of $\frac{u}{U_\infty}$ at $\frac{x}{c} = 0.5$. Left: $M_\infty = 0.4$; Right: $M_\infty = 0.8$. Experimental data from Ref. [9-12].

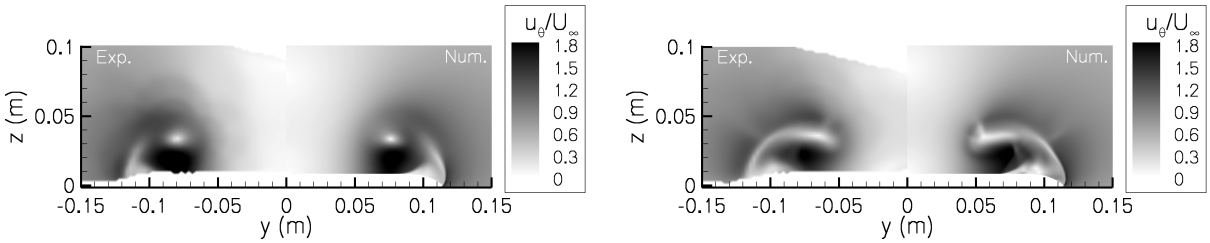

(a) (b)

Figure 5: Numerical and experimental contours of $\frac{u_\theta}{U_\infty}$ at $\frac{x}{c} = 0.5$. Left: $M_\infty = 04$; Right: $M_\infty = 0.8$. Experimental data from Ref. [9-12].

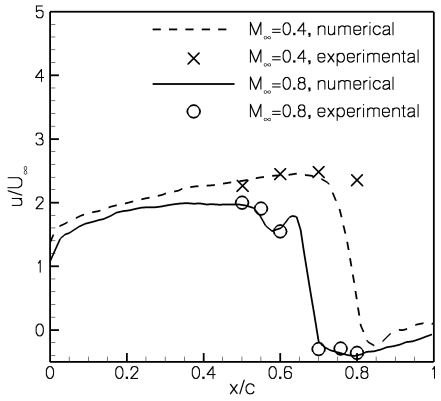

Figure 6: Numerical and experimental evolution of the longitudinal velocity $\frac{u}{U_\infty}$ in the leading-edge vortex for the two cases. Dashed line: $M_\infty = 0.4$; Solid line: $M_\infty = 0.8$. Experimental data from Ref. [9-12].

the leading-edge vortex core is characterized by an almost constant evolution of the longitudinal velocity for the transonic case whereas the longitudinal flow is still accelerated in the subsonic one. It results then in a higher value of $\frac{u}{U_\infty}$ in the subsonic case than in the other one, the maximal value of this ratio being respectively equal to 2.4 and 1.8. The behavior of the two curves is quite different downstream from $\frac{x}{c} = 0.55$. Whereas the flow is still accelerated in the subsonic case, a first decrease of the longitudinal velocity occurs around this position for $M_\infty = 0.8$. Then, the flow is re-accelerated from $\frac{x}{c} = 0.6$ to 0.65 and finally quickly decreases to reach negative values, characterizing the vortex breakdown, around $\frac{x}{c} = 0.7$. The vortex breakdown only occurs around $\frac{x}{c} = 0.8$ in the subsonic case. It has been demonstrated in Ref. [23] that this earlier breakdown in the transonic regime is the consequence of a shock/leading-edge vortex interaction.
Finally, it should be mentionned here that these results are in a good agreement with the experimental observations, in spite of the fact that, for $M_\infty = 0.4$, the vortex breakdown occurs further than $\frac{x}{c} = 0.8$ in experiments. The earlier breakdown numerically observed at $M_\infty = 0.4$ may be explained by the fact that the wind tunnel is not taken into account in the computations [24]. Furthermore, it should be noted that the occurrence of the vortex breakdown is usually experimentally observed over delta wings for such angles of attack and sweep angles in the subsonic regime [25].

5 Study of the cross-flows

5.1 Identification of the cross-flow shock waves in the transonic regime

In the transonic regime, some cross-flow shock waves appear. These shock waves are present around the leading-edge vortex and on the top of the shear layer. In the current case, five cross-flow shock waves are identified, as presented in figure 7 showing the contours of the averaged transverse Mach number M_{2d} at $\frac{x}{c} = 0.5$. M_{2d} is the Mach number based on the lateral and vertical velocity components.

In conformity with the observations of Donohoe *et al.* [26], the shock number 1 located

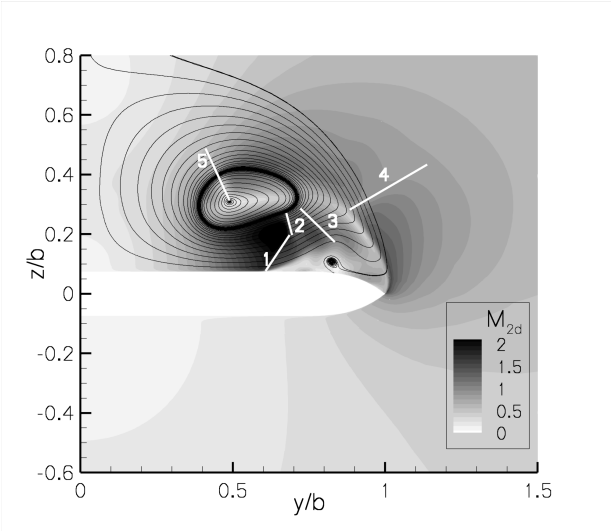

Figure 7: Contours of the cross-flow Mach number M_{2d} at $\frac{x}{c} = 0.5$ and pseudo-streamlines for the transonic case: Identification of the cross-flow shock waves.

beneath the leading-edge vortex is caused by the acceleration of the cross-flow in this region. The four other shock waves are likely to be caused by the curvature of the trajectory of the flow causing the flow to accelerate up to thermophysical conditions which cannot be sustained.

5.2 Displacement of the vortex core

In order to study the leading-edge vortex dynamic, figures 8 and 9 show the Probability Density Functions (PDF) of both lateral and vertical locations of the vortex core for the two considered Mach numbers.

In these figures, the PDF resulting from the present simulations appear in continuous line and a Gaussian distribution based on the mean value and on the standard deviation

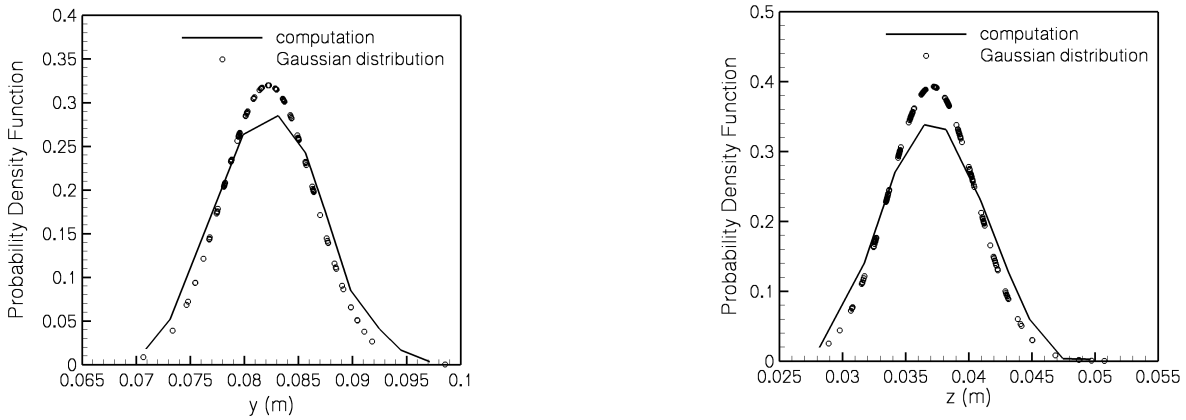

(a) (b)

Figure 8: Probability Density Function of the location of the leading-edge vortex core at $\frac{x}{c} = 0.5$ in the subsonic case. Left: lateral location; Right: vertical location.

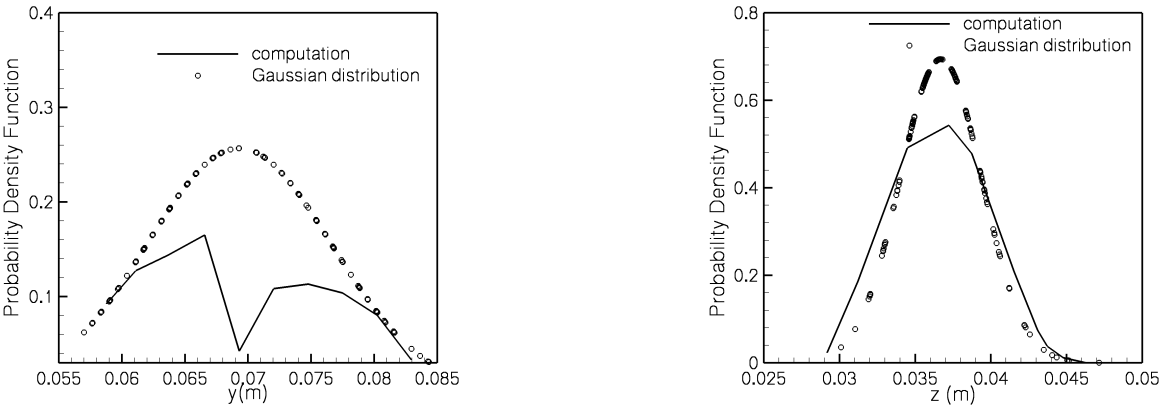

(a) (b)

Figure 9: Probability Density Function of the location of the leading-edge vortex core at $\frac{x}{c} = 0.5$ in the transonic case. Left: lateral location; Right: vertical location.

of each signal is also represented (symbols).
One can notice that the PDF of the lateral and normal locations are similar to a Gaussian distribution. It can be linked to the experimental observations of Menke and Gursul [27] who showed that the PDF of the swirl velocity close to the leading-edge vortex core

presents such a shape.
Concerning the transonic case, one can observe in figure 9 that the PDF of the normal displacements of the leading-edge vortex core is still close to a Gaussian Distribution, an increase of the freestream Mach number having no consequence on the movement in the vertical direction.

However, the situation is different for the transverse location, since the PDF of $y(t)$ presents two large-band peaks centered on $y = 0.065$ and $y = 0.075$. It has been demonstrated in Ref [23] that this motion find its origin in the interaction of the crossflow shock beneath the main vortex and the boundary layer developing on the suction side of the wing.

6 Control of the vortical flow in the transonic regime

6.1 Introduction

Control of vortical flow over delta wings in the subsonic regime has been the subjet of many investigations in recent years. The main control approaches that have been investigated are the following:

- Blowing at the trailing edge of the wing [28, 29];
- Suction/blowing at the leading-edge [30, 31, 32];
- Blowing in the vortex core [33, 34].

Even if these approaches are efficient to delay the occurrence of the vortex breakdown in the subsonic regime, their potential efficiencies are unknown in the transonic regime. Thus, the purpose of this study is to numerically evaluate continuous suction effects on the dynamic of the leading-edge vortex and on the aerodynamic performances of the wing in the transonic regime.

6.2 Presentation of the control strategy

The suction slot is located at the leading-edge of the wing, from its apex to $\frac{x}{c} = 0.8$. This later position is downstream from the location of the vortex breakdown in the reference case (see Figure 10). The suction velocity is $U_{slot} = 170\ m.s^{-1}$. It corresponds to a value of the momentum coefficient $C_\mu = \frac{\rho_{slot} S_{slot} U_{slot}^2}{0.5 \rho_\infty S_{wing} U_\infty^2}$ equal to 2%. In this equation, S_{slot} and S_{wing} are respectively the surface of the suction slot and of the wing and ρ_{slot} is the density imposed in the slot.
It should be mentioned here that control strategies based on blowing at the leading-edge of the wing and in the vortex core have also been evaluated. Nevertheless, it appears that with such a value of C_μ, the blowing velocity is not high enough to disturb the flow in the leading-edge vortex and these computations are not presented in this paper.

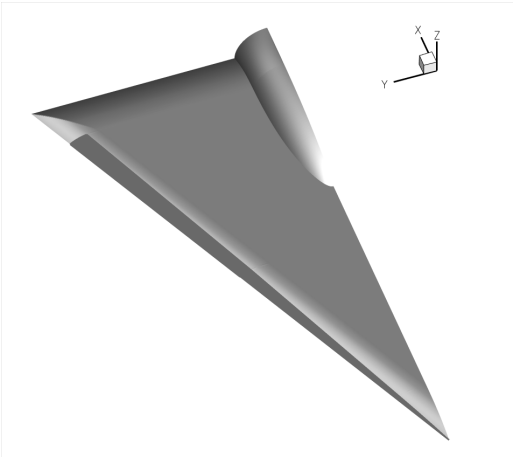

Figure 10: Representation of the VFE-2 geometry and of the suction slot (dark).

7 Instantaneous flow

Figure 11 shows contours of $|grad(\rho)|$ in a transverse plane at $\frac{x}{c} = 0.5$. As depicted in this figure, applying a suction at the leading-edge of the wing deeply alters the flow topology.
In the controlled case, one can observe that the cross-flow shock observed in the reference case beneath the leading-edge vortex is no longer present and is substituted by an oblique shock sitting on the suction slot. Another fundamental observation is that the secondary vortex does not appear anymore in the suction case. Finally, the leading-edge vortex is closer to the wing than in the reference case.

8 Suction effects on the dynamic of the vortical flow

8.1 Overview on the cross-flow topology in the controlled case

As it has been just presented, an oblique shock sits on the suction slot in the controlled case. Thus this section characterizes its properties. To this end, we will focus now on the topology in a plane perpendicular to the leading-edge of the wing. The velocity components in the (Ox'y'z') reference are then:

$$u' = u \times cos(\phi) - v \times sin(\phi); \quad v' = u \times sin(\phi) + v \times cos(\phi); \quad w' = w \tag{1}$$

Where ϕ is the sweep angle of the wing.
Figure 12 shows contours of the normal Mach number M_n and the streamlines in a plane perpendicular to the leading-edge of the wing in the suction case.
Streamlines downstream from the cross-flow shock are subjected to two deviations. The first one, θ, occurs right after the shock and can classically be evaluated as following:

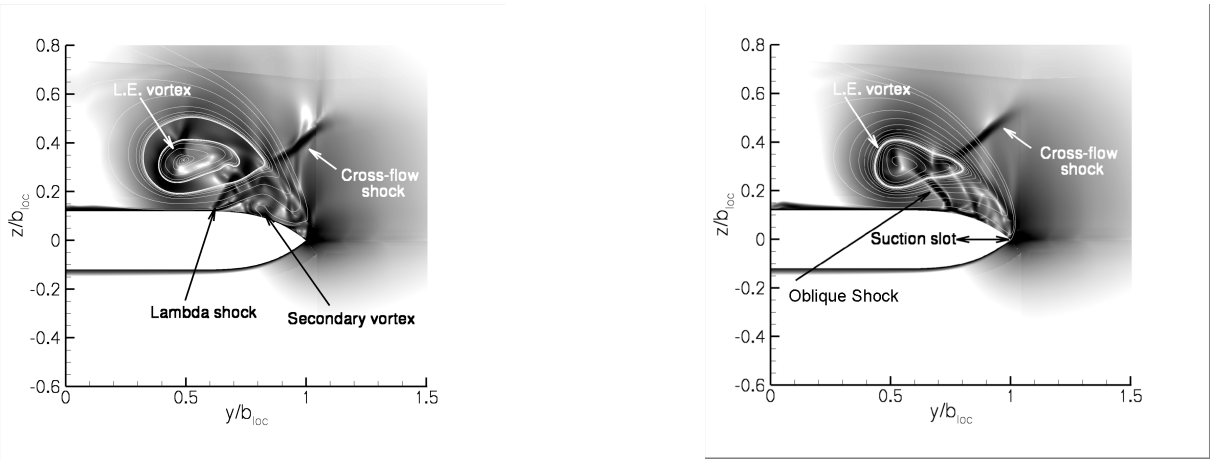

(a) (b)

Figure 11: Contours of $|grad(\rho)|$ at $\frac{x}{c} = 0.5$. Left: Reference case; Right : With suction.

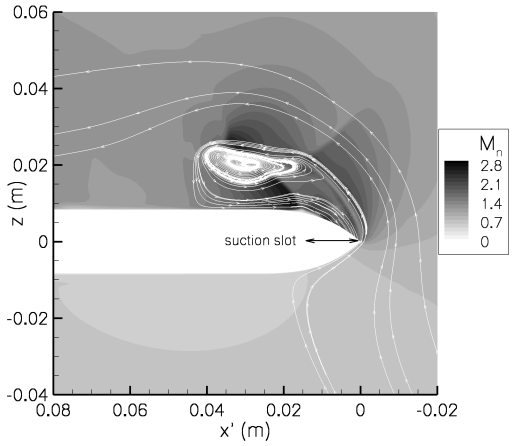

Figure 12: Contours of the normal Mach number and streamlines in a plane perpendicular to the leading-edge of the wing.

$$\frac{tg\,(\sigma - \theta)}{tg\,(\sigma)} = \frac{\rho_0}{\rho_1} \tag{2}$$

Where ρ_0 and ρ_1 are respectively the density upstream and downstream of the shock and σ is the angle between the shock and the horizontal part of the suction side of the wing. This equation gives a value of θ equals to 17°, which is quite close to the value of 15° observed in the computation.

Finally, the second deviation, of about 35°, toward the suction side of the wing is directly induced by the suction.
Thus, the cross-flow topology in the controlled case highly differs from the one in the reference case. The main modifications are the displacement of the cross-flow shock toward the leading-edge of the wing, the suppression of the shock/boundary layer interaction and of the secondary vortex and an important deviation of the cross-flow toward the wing.

8.2 Lateral dynamic of the vortical flow

In order to evaluate suction effects on the dynamic of the vortical flow, Figure 13 shows the Probability Density function (PDF) of the lateral location of the shock and of the leading-edge vortex core at $\frac{x}{c} = 0.5$.
In the controlled case, the PDF exhibits a single sharp peak which attests of the suppression of the sinusoidal motion. As a consequence, the leading-edge vortex is stabilized, that is characterized by the single peak in the PDF of its lateral location. However, it should be noted here that this peak is less acute than what is observed in the PDF of the location of the shock since the vortex is still influenced by instabilities embedded in the shear layer emanating from the leading-edge of the wing.
This lateral stabilization of the leading-edge vortex leads to a reduction of the fluctuating

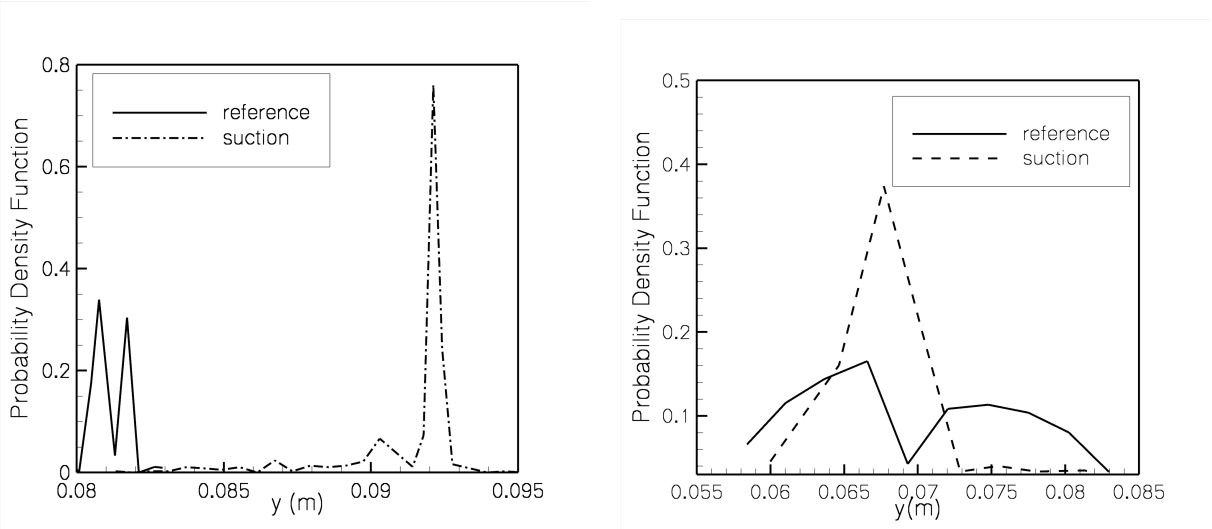

(a) (b)

Figure 13: Probability Density function of the lateral location of the shock (Left) and of the leading-edge vortex core (Right).

kinetic energy, as depicted by Fig 14 showing the contours of $\frac{k}{U_\infty^2}$ in a plane cutting the

vortex core.

In fact, one can observe that from the apex of the wing to the vortex breakdown location,

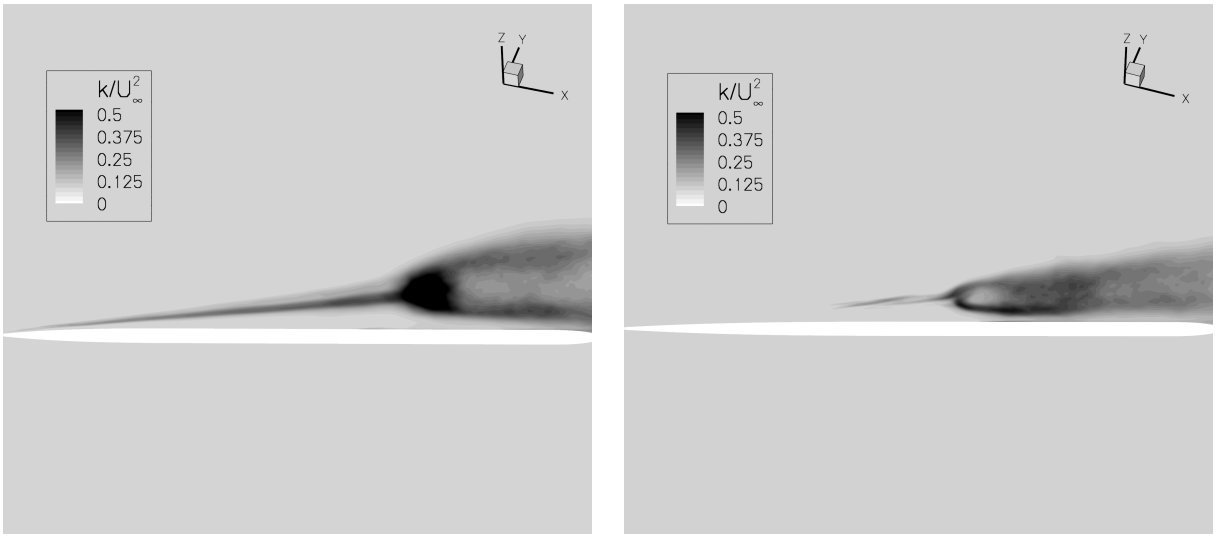

(a) (b)

Figure 14: Contours of $\frac{k}{U_\infty^2}$ through the vortex core. Left: Reference case; Right: With suction.

levels of $\frac{k}{U_\infty^2}$ significantly decrease in the suction case in comparison with the reference one. Levels of k are then divided by two. Eventually, the vortex breakdown occurs, highlighted by a brutal increase of the turbulent kinetic energy. However, this augmentation is less important in the suction case than in the reference one, the maximal values of $\frac{k}{U_\infty^2}$ being respectively equal to 0.38 and 0.5.

9 Suction effects on the aerodynamic performances of the wing

To conclude this study, this section focuses on the suction effects on the aerodynamic performances of the wing. As a starting point, Figure 15 presents the spanwise distribution of the pressure coefficient C_p as a function of $\frac{z}{b_{loc}}$, where b_{loc} is the local half span, for the two considered cases.

It appears in this figure that, whatever the considered longitudinal location, the pressure coefficient decreases when the suction is applied at the leading-edge of the wing. In particular, this decrease reaches 23% at $\frac{x}{c} = 0.2$ and 0.5. At the rear of the suction slot ($\frac{x}{c} = 0.8$), this decrease of C_p is less intense and approximately equals 12%. This decrease of pressure on the suction side originates from two sources: the displacement of the leading-edge vortex towards the wall and the acceleration of the cross-flow induced by

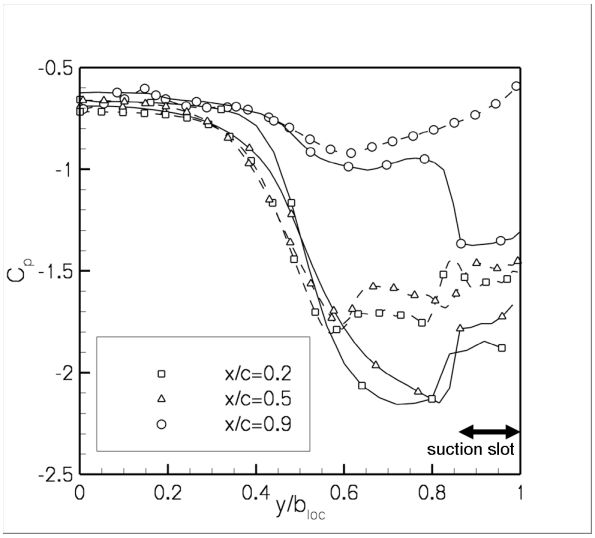

Figure 15: Spanwise distribution of the pressure coefficient C_p. Dashed lines: Reference case; Solid lines: Suction case.

the suction. It results in an increase of the lift coefficient of 22%. Moreover, a decrease of 9% of the drag coefficient is observed.
Finally, the previously suction-induced stabilization of the vortical flow leads to a decrease of the loading fluctuations of 20%.

10 Conclusion

The compressibility effects on the vortical flow developing over a 65° swept delta wing placed at an angle of attack equal to 25.5° has been first investigated by computing the flow over the VFE-2 delta wing with two freestream Mach numbers equal to 0.4 and 0.8. These computations are based on a turbulent modeling coupling DDES and ZDES approaches, allowing a faster decay of the eddy-viscosity in LES regions than with the DDES method.
The study of the time-averaged cross-flow in some transverse planes underlines the presence of five cross-flow shocks all around the vortical flow. In particular, a cross-flow shock wave sits in the region between the suction side of the wing and the external edge of the leading-edge vortex. It is shown in this study that the cross-flow shock periodically moves in the lateral direction.
Owing to this shock unsteadiness, the behavior of the leading-edge vortex is altered for $M_\infty = 0.8$. The Probability Density Function (PDF) of the lateral movement of the vortex core in the subsonic case is approximately Gaussian. Nevertheless, in the transonic case, this PDF is coupled with the one of the signal resulting from the periodic lateral movement of the cross-flow shock beneath the leading-edge vortex. It should be noted

that parallel to this, the PDF of the movement in the normal direction are approximately Gaussian for the two Mach numbers.
Then, suction effects in the transonic regime have been investigated. The suction slot is located at the leading-edge of the wing and the momentum coefficient has been set equal to 2%. It has been demonstrated that suction deeply alters the cross-flow topology. In particular, suction moves the leading-edge vortex toward the upper side of the wing and removes both the secondary vortex and the cross-flow shock beneath the leading-edge vortex. This later is replaced by an oblique shock which sits on the slot. It has been demonstrated in the suction case that this shock is not subject to a lateral instability, contrary to what is observed in the reference case. Consequently, the absence of lateral instability stabilizes the whole vortical flow and then decreases the turbulent kinetic energy in the main vortex. As a result, aerodynamic loading fluctuations are decreased by 20%.

Acknowledgments

The authors would like to acknowledge the DGA (French Ministry of Defense) for its financial support and would like to thank Robert Konrath of the DLR Gottingen for having kindly provided the access to the experimental data.

REFERENCES

[1] M. Elsayed, F. Scarano, and N.G. Verhaagen. Leading-Edge Shape Effect on the Flow over Non-Slender Delta Wings. *AIAA Paper, No. 2008-344, Reno, January*, 2008.

[2] J.M. Luckring. Reynolds Number and Leading-Edge Bluntness Effects on a 65° Delta Wing. *AIAA Paper, No. 2002-0419, Reno, January*, 2002.

[3] R.M. Cummings and A. Schütte. Detached-Eddy Simulation of the Vortical Flowfield about the VFE-2 Delta Wing. *AIAA Paper, No. 2008-396, Reno, January*, 2008.

[4] A.M. Mitchell. Caractérisation et contrôle de l'éclatement tourbillonnaire sur une aile delta aux hautes incidences. *Ph.D. thesis*, University Paris 6, France, 2000.

[5] F. Renac. Contrôle expérimental de l'écoulement tourbillonnaire sur une aile delta. *Ph.D. thesis*, University Paris 6, France, 2004.

[6] E.C. Polhamus. A concept of the vortex lift of sharp-edged delta wings based on a leading-edge-suction analogy. Technical Report TN-D-3767, NASA, 1971.

[7] M. Escudier. Vortex breakdown: observations and explanations. *Progress in Aerospace Sciences*, **25**, 189–229, 1988.

[8] D. Hummel and G. Redeker. A new vortex flow experiment for computer code validation. *RTO-MP-069(1)*, 2001.

[9] R. Konrath, C. Klein, R.H. Engler and D. Otter. Analysis of PSP results obtained for the VFE-2 65 degree delta wing configuration at sub- and transonic speeds. *AIAA Paper No. 06-60, Reno, January*, 2006.

[10] R. Konrath, A. Schroder and J. Kompenhans. Analysis of PIV results obtained for the VFE-2 65 degree delta wing configuration at sub-and transonic speeds. *AIAA Paper No. 06-3003, Reno, January*, 2006.

[11] R. Konrath, C. Klein and A. Schroder. PSP and PIV investigations on the VFE-2 configuration in sub- and transonic flow. *AIAA Paper No. 2008-379, Reno, January*, 2008.

[12] A. Schroder, J. Agocs, H. Frahnert, D. Otter and H. Mattner. Application of stereo PIV to the VFE-2 65 degree delta wing configuration at sub- and transonic speeds. *AIAA Paper No. 2006-3486, Reno, January*, 2006.

[13] M. Pechier, Prévisions numériques de l'effet Magnus pour des configurations de munition. *Ph.D. thesis, University Paris 6*, 1999.

[14] C.W. Gear. Algorithm 407-DIFSUB for the solution of ordinary differential equations. *Commun. ACM*, 14: 185–190, 1971.

[15] I. Mary and P. Sagaut. Large Eddy Simulation of the flow around an airfoil near stall. *AIAA J.*, 40(6): 1139–1146, 2002.

[16] P.R. Spalart, S. Deck, M.L. Shur, K.D. Squires, M.K. Strelets and A. Travin. A new version of Detached-Eddy Simulation, resistant to ambiguous grid densities. *Theoret. Comput. Fluid Dynamics*, 20: 181–195, 2006.

[17] S. Deck. Zonal Detached Eddy Simulation of the flow around a high lift configuration. *AIAA J.*, 43(11): 2372–2384, 2005.

[18] P.R. Spalart and S.R. Allmaras. A one-equation turbulence model for aerodynamic flows. *AIAA Paper No. 92-04339, Reno, January*, 1992.

[19] J. Riou, E. Garnier, S. Deck and C. Basdevant. An improvement of Delayed Detached Eddy Simulation applied to a separated flow over a missile fin. AIAA J., 47(2): 345–360, 2009.

[20] N.T. Clemens and M.G. Mungal. Large-scale structure and entrainment in the supersonic mixing layer. *J. Fluid Mech*, 284: 171–216, 1995.

[21] G.E. Erickson and L.W. Rogers. Experimental study of the vortex flow behavior on a generic fighter wing at subsonic and transonic speeds. *AIAA Paper No. 87-1262, Honolulu, June*, 1987.

[22] G.E. Erickson, J.A. Schreiner and L.W. Rogers. Multiple vortex and shock interaction at subsonic, transonic and supersonic speeds. *AIAA Paper No. 90-3023, Portland, August*, 1990.

[23] J. Riou, E. Garnier and C. Basdevant. Compressibility effects on the vortical flow over a 65 degrees delta wing. *Phys. Fluids*, 22, 035102, 2010.

[24] R. Konrath. *Private communication.*

[25] A. Pelletier and R.C. Nelson. An experimental study of static and dynamic vortex breakdown on slender delta wing planforms. *AIAA Paper No.94-1879*, 1994.

[26] S.R. Donohoe and W.J. Bannink. Surface reflective visualizations of shock-wave/vortex interactions above a delta wing. *AIAA J.*, 35(10): 1568–1573, 1997.

[27] M. Menke and I. Gursul. Unsteady nature of leading-edge vortices. *Phys. Fluids*, 9(10):2960–2966, 1997.

[28] Helin, H.E., Wattry, C.W., "Effects of leading-edge jet entrainment on delta wings vortices," *AIAA J.*, 32(4): 802-804, 1994.

[29] Vorobieff, P.V., Rockwell, D.O., "Multiple-actuator control of vortex breakdown on a pitching delta wing," *AIAA J.*, 34(10): 2184-2186, 1996.

[30] Renac, F., Barberis, D., Molton, P., "Control of vortical flow over a rounded leading-edge delta wing," *AIAA J.*, 47(7): 1409-1418, 2005.

[31] Guy, Y., Morrow, J.A., McLaughlin, T.E., "Velocity measurements on a delta wing with periodic blowing and suction," *38th AIAA Aerospace Sciences Meeting and Exhibit*, 2000-0550, 2000.

[32] Guy, Y., Morrow, J.A., McLaughlin, T.E., "Numerical investigation of the flowfield on a delta wing with periodic blowing and suction," *38th AIAA Aerospace Sciences Meeting and Exhibit*, 2000-33797, 2000.

[33] Kuo, C.H., Lu, N.Y., "Unsteady vortex structure over delta-wing subject to transient along-core blowing," *AIAA Journal*, 36(9): 1658-1664, 1998.

[34] Kuo, C.H., Lu, N.Y., Lin, D.C., "Evolution of vortical structure over delta wing with transient along-core blowing," *AIAA Journal*, 33(4): 617-624, 1997.